

Genuine Phase Diagram of Homogeneously Doped CuO_2 Plane in High- T_c Cuprate Superconductors

Hidekazu Mukuda¹, Yuhei Yamaguchi¹, Sunao Shimizu¹, Yoshio Kitaoka¹, Parasharam Shirage², Akira Iyo²

¹Graduate School of Engineering Science, Osaka University, Toyonaka, Osaka 560-8531

²National Institute of Advanced Industrial Science and Technology (AIST), Umezono, Tsukuba 305-8568

We report a genuine phase diagram for a disorder-free CuO_2 plane based on the precise evaluation of the local hole density (N_h) by site-selective Cu-NMR studies on well-layered high- T_c cuprates. It has been unraveled that (1) the antiferromagnetic metallic state (AFMM) is robust up to $N_h \approx 0.17$, (2) the uniformly mixed phase of superconductivity (SC) and AFMM is realized at $N_h \approx 0.17$, (3) the tetracritical point for the AFMM / (AFMM + SC) / SC / PM (Paramagnetism) phases may be present at $N_h \approx 0.15$ and $T \approx 75$ K, (4) T_c is maximum close to a quantum critical point (QCP) at which the AFM order collapses, suggesting the intimate relationship between the high- T_c SC and the AFM order. The results presented here strongly suggest that the AFM interaction plays the vital role as the glue for the Cooper pairs, which will lead us to a genuine understanding of why the T_c of cuprate superconductors is so high.

KEYWORDS: superconductivity, copper-oxide, antiferromagnetism, NMR, phase diagram

1. Introduction

Despite of more than 22 years of research, there is still no universally accepted theory for mechanism of cuprate superconductors. The high- T_c superconductivity (SC) in cuprates emerges on a CuO_2 plane when an antiferromagnetic (AFM) Mott insulator is doped with mobile carriers. A strong relationship between AFM order and SC is believed to be a key to understand the origin of their remarkably high SC transition.¹⁽⁵⁾ Experimentally, however, in a prototype high- T_c cuprate $\text{La}_{2-x}\text{Sr}_x\text{CuO}_4$ (LSCO), the AFM and SC phases are separated by the spin-glass phase in association with the carrier localization.⁶⁾ Since chemical substitution is necessary for doping, a disorder ect poses a significant and inevitable problem in doped cuprates generally. Multilayered cuprates provide us with the opportunity to research the characteristics of the disorder-free CuO_2 plane. Figure 1(a) shows the crystal structure of the Hg-based well-layered cuprate $\text{HgBa}_2\text{Ca}_4\text{Cu}_5\text{O}_{12+}$ (Hg-1245) composed of two types of CuO_2 planes in a unit cell: a pyramid-type outer CuO_2 plane (OP) and a square-type inner plane (IP).⁷⁾ The site-selective NMR is the best and the only tool used to extract layer-dependent characteristics.⁸⁽¹²⁾ Since the IPs are farther from the charge reservoir layers (HGO) than the OPs, the carrier density at IPs is lower than that at OPs. The disorder introduced along with the chemical substitution in an HGO layer is effectively shielded on an OP, as a result of which ideally at CuO_2 planes are realized, especially at IPs, differentiating multilayered cuprates from mono-layered cuprate LSCO. In particular, the uniform mixing state of SC and AFM order on an OP for underdoped Hg-1245 has been shown in a previous study;¹¹⁾ however, the carrier density and Neel temperature inherent in this layer have not been identified.

In this paper, we have revealed the intrinsic phase di-

agram of a disorder-free CuO_2 plane on the basis of the site-selective Cu-NMR studies on Hg-based well-layered cuprates. The most remarkable feature of this phase diagram is that the AFM metallic phase is robust and coexists with the SC phase in a region extending up to the optimally doped region. T_c has a peak close to a quantum critical point at which the AFM order collapses, suggesting the intimate relationship between AFM order and SC. Our findings imply that the AFM interaction plays the vital role as the glue for the Cooper pairs.

2. Experimental

A polycrystalline sample of Hg-1245 (OPT)2 has been synthesized at a pressure (temperature) of 2.5 GPa (950 C), which is lower than that applied in the sample synthesis in the previous studies,^{10,13)} i.e., 4.5 GPa (1050 C), and referred to as "Hg-1245 (OPT)1" in this study. The SC transition temperature T_c has been determined to be 110 K from the onset of a sharp diamagnetic signal in dc susceptibility. For the NMR measurements, we used oriented powder samples aligned along the c-axis under a high magnetic field. The narrow linewidths in the Cu NMR spectra, particularly those less than 50 Oe for IPs even at 15 T (Hkc), indicate disorder-free CuO_2 planes that are homogeneously doped, which enables us to precisely measure the Knight shift.

3. Results

3.1 Superconducting property of Hg-1245 (OPT)2

Figure 1(b) shows temperature dependence of field swept ^{63}Cu NMR spectra obtained at a fixed frequency of 174.2 MHz in the field perpendicular to the c-axis. The ^{63}Cu -NMR signals from OP and IP are separately observed due to the difference of the Knight shift and nuclear quadrupole shift.¹⁰⁾ The narrow linewidths in the Cu NMR spectra, particularly for IPs, indicate disorder-free CuO_2 planes that are homogeneously doped, and also imply that the disorder introduced along with the

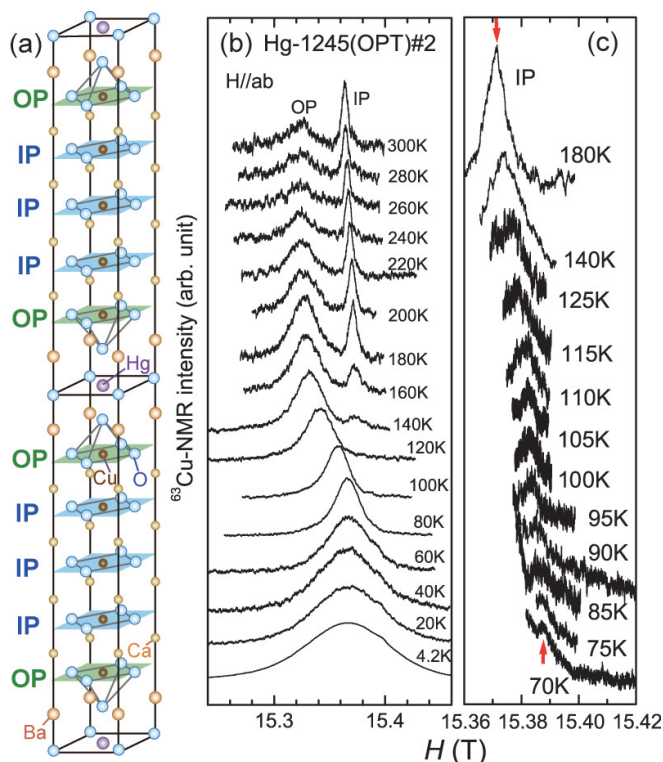


Fig. 1. (Color online) (a) Crystal structure of ve-layered Hg-1245. (b) Temperature dependence of ^{63}Cu -NMR spectra of Hg-1245(OPT)2. The ^{63}Cu -NMR signals from a pyramid-type outer CuO_2 plane (OP) and a square-type inner plane (IP) are separately observed due to the difference of the Knight shift and nuclear quadrupole shift. The narrow linewidths in the Cu NMR spectra, particularly for IP s, indicate disorder-free CuO_2 planes that are homogeneously doped. It should be noted that the resonance peak of IP disappears below 130K due to the short nuclear spin-spin relaxation time T_2 at IP site. (c) However, in the appropriate pulse condition, we can detect the extremely small resonance signal of IP down to 70K, which enables us to determine Knight shift for IP between 70 K and 300 K.

chemical substitution in an HgO layer is effectively shielded on an OP. It should be noted that the resonance peak of IP disappears below 130K, as shown in Fig.1 (b), due to the short nuclear spin-spin relaxation time T_2 at IP site. However, in the appropriate pulse condition that the interval of the $\pi/2$ pulse is as short as 3.4 μs , we succeeded in detecting the extremely small resonance signal of IP down to 70K, as shown in Fig. 1 (c), which enables us to determine Knight shift for IP between 70 K and 300 K.

The Knight shift generally consists of spin and orbital components denoted as K_s and K_{orb} , respectively. Figure 2 shows the temperature (T) dependences of K_s^{ab} (K_s^{ab} in a field parallel to the ab-plane) for OPs and IP s of Hg-1245(OPT)2, respectively. Here, K_s^{ab} is obtained by subtracting temperature-independent K_{orb}^{ab} , which is approximately 0.2-0.21%, irrespective of IP or OP for Hg-based cuprates.^{14,15} K_s^{ab} of OP s decreases rapidly below $T_c = 110$ K. We note that a distinct peak in the temperature derivatives of K_s^{ab} (OP) coincides with $T_c = 110$ K. On the other hand, K_s^{ab} (IP) decreases significantly at $T < 85$ K in addition to its observed decrease at bulk T_c of 110 K, which has been corroborated by the two

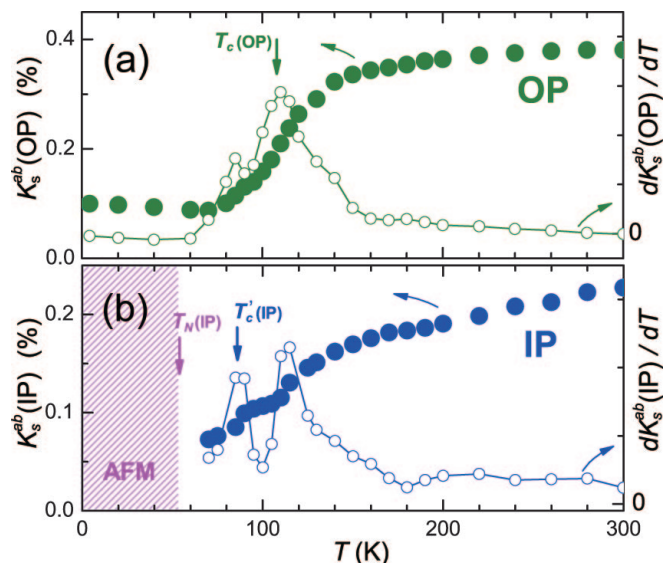


Fig. 2. (Color online) Temperature dependence of K_s^{ab} for (a) OP and (b) IP of Hg-1245(OPT)2. The solid and empty circles represent K_s and its temperature-derivatives, respectively. K_s^{ab} (OP) decreases rapidly below $T_c = 110$ K, whereas K_s^{ab} (IP) decreases significantly at $T = 85$ K. This indicates that although the bulk SC transition is driven primarily by OPs, the SC gap in IP s rapidly develops below $T'_c(\text{IP}) = 85$ K, that is inherent T_c of IP s.

peaks at 85 and 110 K in the temperature derivatives of K_s^{ab} (IP). This result reveals that the bulk SC transition is driven primarily by an optimally doped OP, but the SC transition inherent in underdoped IP s manifests itself at $T'_c(\text{IP}) = 85(5)$ K due to a large imbalance in the carrier densities between OPs and IP s. It is naturally expected that IP s exhibit superconductivity between 85 and 110 K due to the proximity effect, which has been observed in other multilayered cuprates.^{8,9} The analogous behavior was also observed in slightly overdoped Tl-1245(OVD) with $T_N = 45$ K,¹⁰ in which the SC transition inherent in IP s is $T'_c(\text{IP}) = 90(5)$ K, whereas the bulk SC transition at 100 K is driven primarily by OPs, as shown in Fig. 3. As discussed in section 3.3, it is reasonable that T_N is lower and T_c is higher than those of Hg-1245(OPT)2, since the carrier density of IP s is slightly higher than that for Hg-1245(OPT)2.

3.2 Magnetic property of Hg-1245(OPT)2

As presented in Fig. 1 (c), the NMR signal of IP s of Hg-1245(OPT)2 disappears below 70 K because of the extremely short relaxation time due to the development of critical AFM spin fluctuations towards a possible Neel ordering T_N even in the SC state. Generally a peak of nuclear-spin relaxation rate $1/T_1$ is observed at T_N due to critical slowing down. In fact, as shown in Fig. 4, $T_N = 55$ K has been confirmed by a peak in a plot of $1/T_1$ versus T at an OP. The onset of the AFM order at IP s has been evidenced by the zero-field (ZF) Cu NMR spectrum at 1.5 K without any external field, as shown in Fig. 5. The peak at 15 MHz has been attributed to OPs in the paramagnetic state because the peak almost coincides with the nuclear quadrupole resonance (NQR)

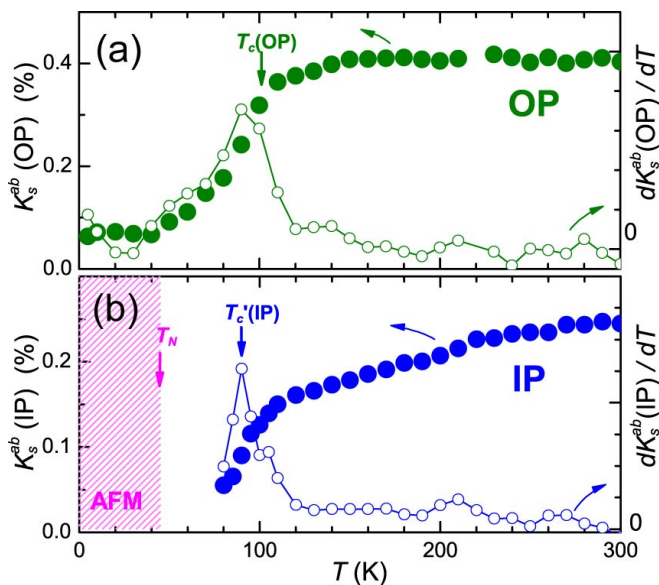


Fig. 3. (Color online) Knight shift (K_s^{ab}) measurement for (a) OP and (b) IP of slightly overdoped Tl-1245 (OVD) with $T_c = 100$ K. The solid and empty circles represent K_s and its temperature derivatives, respectively. In this study, we have detected small resonance signal of IP down to 80 K in the appropriate pulse condition. It has been found that the SC transition inherent in IP takes place at $T_c'(IP) = 90(\pm 5)$ K, and the bulk SC transition at 100 K is driven primarily by OPs. The AFM order emerges at IPs below $T_N = 45$ K¹⁰⁾ with a moment of $M_{AFM}(IP) = 0.1 \mu_B$, whereas the OP is nearly paramagnetic.¹¹⁾

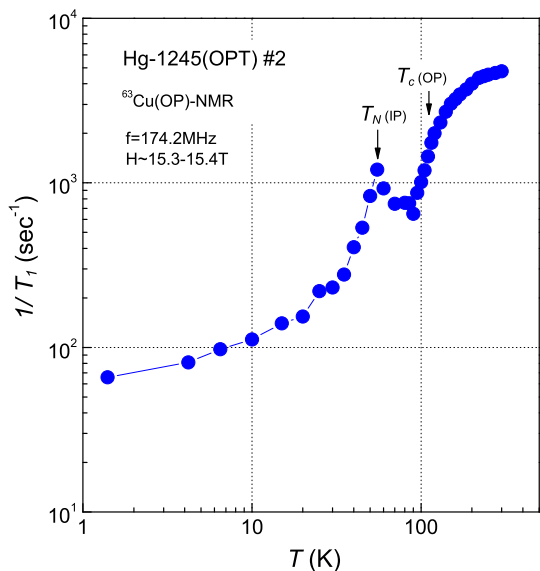


Fig. 4. (Color online) Nuclear-spin relaxation rate $1/T_1$ for the OPs of Hg-1245(OPT) #2. The Neel temperature $T_N = 55$ K at IP has been identified by a distinct peak due to the critical slowing down in the plot of $1/T_1$ versus T at OP. Similarly, in a previous paper,¹⁰⁾ T_N for Hg-1245(OPT) #1 and Tl-1245(OVD) has been identified to be 60 and 45 K, respectively. Here, as for in the SC state, the short component of T_1 is plotted in the figure since it is sensitive to the magnetic order at IP s.¹⁰⁾

frequency for OPs, $\nu_Q(OP) = 16$ MHz.¹⁰⁾ The slight shift to lower frequency side may derive from a presence of a tiny field (~ 0.1 T) at the OP due to the proximity effect from IP s. The spectrum of IP s is observed at 23 MHz, not at $\nu_Q(IP) = 8.4$ MHz.¹⁰⁾ The spectral analysis of IP s, assuming a Zeeman field, reveals that an internal field (H_{int}) of 2.0 T is induced by the spontaneous AFM moments $M_{AFM}(IP)$ due to the AFM order at the Cu site in IP s, as displayed by the bars in the figure. The unique value of $M_{AFM}(IP)$ is evaluated to be $0.095 \mu_B$ per Cu site at IP s by using the relation $H_{int}(IP) = \gamma_{hf}(IP) M_{AFM}(IP)$ with the hyperfine coupling constant $A_{hf}(IP) = 20.7$ T = μ_B .¹⁰⁾ It is remarkable that this AFM moment spontaneously emerges at superconducting IP s with a possible commensurate AFM structure. Here, we can exclude the spin-glass state at IP s because the internal field at IP s ($H_{int} = 2.0$ T) is almost the same at all the Cu(IP) sites and its distribution is less than ~ 0.2 T. These results provide the microscopic evidence of the uniform mixing of SC and AFM order on disorder-free IP s with an indisputable moment.

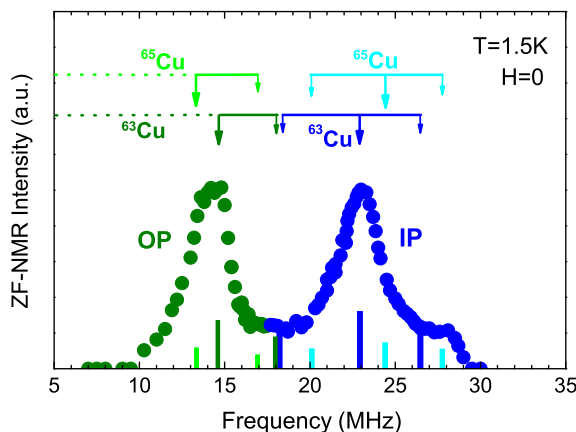


Fig. 5. (Color online) Zero-field Cu NMR spectrum of Hg-1245(OPT) #2 at 1.5 K gives a strong evidence of the onset of the AFM order at IP s. The spectrum around 23 MHz is reproduced by assuming the internal field to be 2.0 T, which is induced by the spontaneous moments ($M_{AFM}(IP) = 0.1 \mu_B$) produced by the AFM order at the Cu sites in IP s. The bars indicate the calculated resonance lines in IP and OP for $^{63};^{65}$ Cu isotopes. The peak at 15 MHz has been attributed to OPs in the paramagnetic state because the peak almost coincides with the NQR frequency for OPs, $\nu_Q(OP) = 16$ MHz.¹⁰⁾ The slight shift to lower frequency side derives from a presence of a tiny field (~ 0.1 T) at the OP due to the proximity effect from IP s.

In the previous study on the Hg-1245(OPT) #1,¹⁰⁾ the AFM moment at IP site of this compound were evaluated to be $0.3-0.37 \mu_B$ from the spectrum analysis between 50-120 MHz (Fig. 6(b)). However, through the systematic NMR investigations on the various multilayered cuprates in the several years, the spectrum between 50-120 MHz has been identified to be the spectrum of the impurity phase, $CaCuO_2(II)$ with a monoclinic structure¹⁶⁾ by comparing the spectrum with that of pure $CaCuO_2(II)$

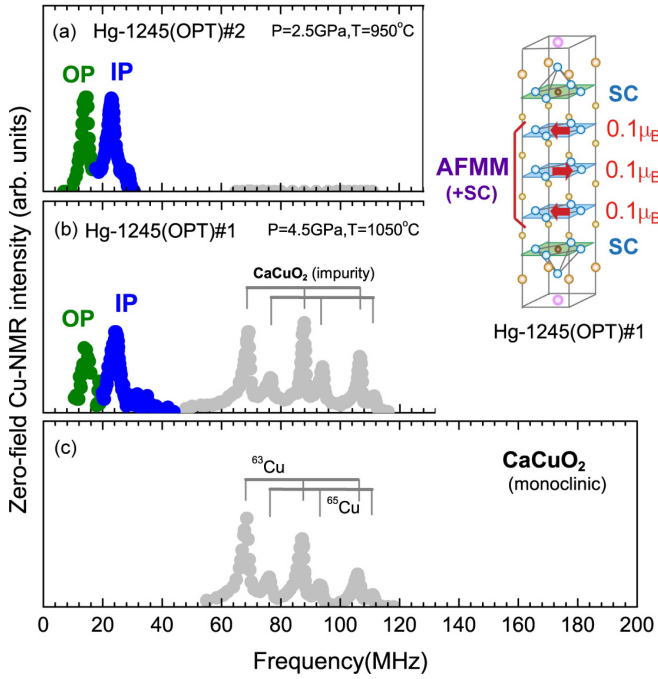


Fig. 6. (Color online) (b) In the previous study on the Hg-1245(OPT)1,¹⁰ the zero-field NMR spectrum between 50-120 MHz were assigned to be IP s, which has AFM moments of 0.3-0.37 μ_B . However, this spectrum has been identified to be the spectrum of the impurity phase, CaCuO₂ (II) with a monoclinic structure¹⁶) by comparing the spectrum with that of (c) pure CaCuO₂ (II) sample. This impurity phase is produced only during the synthesis at a high pressure (high temperature) of 4.5 GPa (1050 C);¹⁶) hence (a) it has not been observed in the present study on Hg-1245(OPT)2 synthesized under a pressure (temperature) of 2.5 GPa (950 C). As a result, the peak at 24 MHz for Hg-1245(OPT)1 is assigned to be IP s with the moment of $M_{AFM}(IP) = 0.1 \mu_B$. This value is comparable to that observed in Hg-1245(OPT)2, which is consistent with that the carrier density of IP s is similar each other.

sample, as shown in Fig. 6 (c). This impurity phase is produced only during the synthesis at a high pressure (high temperature) of 4.5 GPa (1050 C);¹⁶) hence it has not been observed in the present study on Hg-1245(OPT)2 synthesized under a pressure (temperature) of 2.5 GPa (950 C), as indicated in Fig. 6 (a). As a result, the peak at 24 MHz for Hg-1245(OPT)1 is assigned to be IP s with the moment of $M_{AFM}(IP) = 0.1 \mu_B$, and the other peak at 14 MHz is assigned to be OP in the paramagnetic state that is affected by a very tiny field due to the proximity effect from IP s. Thus, we note that the magnitude of $M_{AFM}(IP) = 0.1 \mu_B$ of Hg-1245(OPT)2 is comparable to that not only in Tl-1245(OVD)¹¹) but also in Hg-1245(OPT)1, which is consistent with that the carrier density of IP s is similar each other, as discussed in next section.

3.3 Evaluation of the carrier density

In the previous papers,^{10,11}) the carrier estimation of the underdoped region had remained as a problem, since the $N_h(IP)$ for Hg-1245(OPT)1 was tentatively inferred from the whole carrier density evaluated by Hall coefficient and the $N_h(OP)$ by Knight shift. In this study, we evaluate the local carrier densities N_h for these layers

only from the Knight shift on the basis of the systematic NMR measurements on the various v -layered cuprates. As shown in Fig. 7 (e), it has been established that N_h in various cuprates can be experimentally deduced from the value of K_s^{ab} at room temperature by using the linear relation $N_h = 0.0462 + 0.502K_s^{ab}(RT)$.^{9,17}) Note that this relation is valid for various high- T_c cuprates, irrespective of the type (square or pyramid) and/or number of CuO₂ planes. In fact, the carrier densities at OP s and IP s have been independently evaluated to be $N_h(OP) = 0.236$ and $N_h(IP) = 0.157$ for Hg-1245(OPT)2. We have summarized the physical properties and N_h estimated from the Knight shift of various v -layered cuprates and shown in Figs. 7 (a-f). It has been demonstrated that the AFM ordering takes place at IP s at least in the range of $0.151 < N_h < 0.168$. The values of $M_{AFM}(IP) = 0.1 \mu_B$ are observed for these cuprates, which are significantly reduced by the mobile holes from 0.5-0.7 μ_B in undoped cuprates.^{11,18}) This emphasizes that the AFM metallic (AFM) phase persists at IP s, although the doping level is as high as $N_h < 0.17$. In contrast, the AFM ordering is not observed at IP s with $N_h = 0.169$ in Cu-1245(OVD),⁹) suggesting that a quantum critical point (QCP) exists at $N_h = 0.17$ in the v -layered cuprates.

4. Discussions

4.1 Phase diagram established in v -layered cuprates

We obtained the novel phase diagram by plotting T_N and T_c as functions of N_h evaluated only by Knight shift measurement, as presented in Fig. 8. The characteristic features are summarized as; (1) the AFM metallic state is robust up to $N_h = 0.17$, (2) the uniformly mixed phase of SC and AFM is realized at $0.15 < N_h < 0.17$ at least, (3) the T_c is maximum close to a QCP at which the AFM order collapses, suggesting the intimate relationship between the high- T_c SC and the AFM order. It is noteworthy that the phase diagram for $0.14 < N_h < 0.18$ including the QCP is precisely determined only by homogeneously doped IP s. This result also indicates the presence of a tetracritical point for the AFM / [AFM + SC] / SC / PM (Paramagnetism) phases at $T = 75$ K with $N_h = 0.15$ at zero fields. This is the first observation in the phase diagrams of high- T_c superconductors, although it was recently reported in the heavy-fermion superconductor CeRhIn₅.¹⁹) In such cases, it is noted that the SO(5) theory unifies the AFM and SC states by a symmetry principle and describes their rich phenomenology through a single low-energy effective model⁴) and hence may be applied to describe the quantum phase transition of AFM order and SC involving the tetracritical point.

The phase diagram in Fig. 8 differs significantly from the well-established phase diagrams of mono-layered LSCO and double-layered YBa₂Cu₃O_{6+x} (YBCO), in which the long-range AFM order collapses completely by doping with an extremely small amount of holes of $N_h = 0.02$ ⁶) and 0.055,²⁰) respectively. In fact, we have presented the temperature dependences of K_s^{ab} for underdoped n -layered cuprates, e.g., $n = 2$: YBa₂Cu₃O_{6.63} ($T_c = 62$ K) reported by Takigawa et al.,²¹) $n = 3$: Hg-1223 ($T_c = 115$ K) reported by Julien et al.,¹⁴) and $n = 4$:

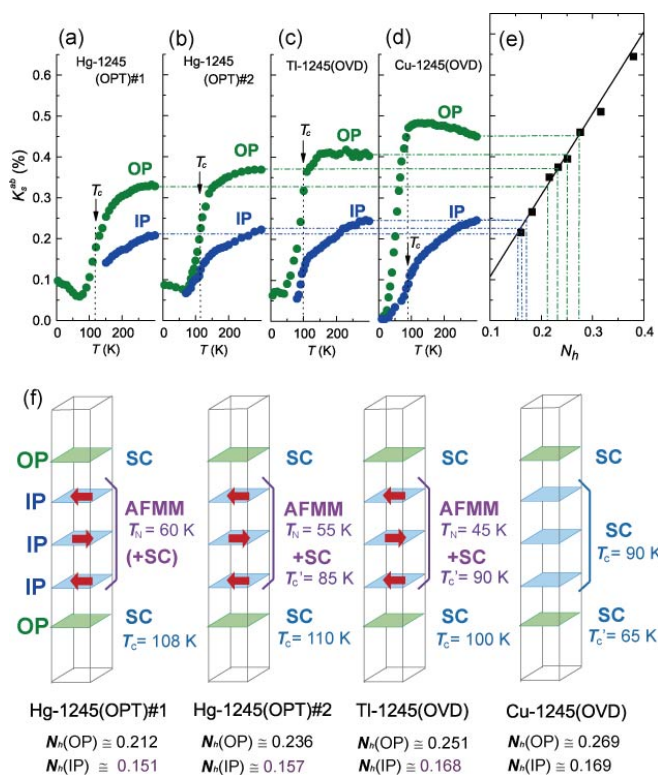


Fig. 7. (Color online) Temperature dependence of K_s^{ab} for (a) Hg-1245(OPT)#1 [cited from Ref.¹⁰], (b) Hg-1245(OPT)#2, (c) Tl-1245(OVD), and (d) Cu-1245(OVD) [cited from Ref.⁹]. (e) K_s^{ab} (RT) at room temperature is proportional to the local carrier density N_h [cited from Refs.^{9,17}], which enables us to estimate N_h for IPs and OPs independently. We have shown that the AFM order spontaneously emerges at disorder-free IPs with $N_h = 0.15-0.168$ below $T_N = 60-45$ K, whereas the SC transition temperature inherent in these layers is T_c (IP) $\approx 85-90$ K. In contrast, the AFM order is not observed in IPs with $N_h > 0.169$ of (d) Cu-1245(OVD), suggesting that a quantum critical point (QCP) exists at $N_h \approx 0.17$ in the ve-layered cuprates. The typical error in N_h is ≈ 0.005 . (f) Layer-dependent physical properties for various ve-layered cuprates are summarized. Here, the value of M_{AFM} (IP) is almost $0.1 \mu_B$ for Hg-1245(OPT)#1, Hg-1245(OPT)#2 and Tl-1245(OVD).

Hg-1234 ($T_c = 110$ K), as shown in Fig. 9. Although their carrier densities are almost the same with N_h (OP or IP) $\approx 0.16-0.01$ evaluated from K_s^{ab} (RT) $\approx 0.22\%$, it should be noted that the ground state remains still in the paramagnetic state for $n = 4$. Although we have investigated two underdoped Hg-1234 samples ($n = 4$) with $T_c = 95$ K and 110 K at N_h (IP) ≈ 0.15 and 0.16 (see Fig. 9(c)), respectively, any static AFM order has not been evidenced at their IPs even though these carrier densities are lower than $N_h = 0.169$ at QCP for ve-layered compounds. Remarkably, the extremely short spin-spin relaxation time was observed in the case of N_h (IP) ≈ 0.15 for underdoped Hg-1234, suggesting the closeness to the QCP of four-layered cuprates. These results strongly suggest that the QCP moves to a region of lower carrier density for n -layered cuprates with $n = 4$, as illustrated in Fig. 10. Although the AFM superexchange interaction among spins at the nearest neighbor Cu sites in a CuO_2 plane is as large as $J_{ab} \approx 1300$ K,²² the effective interlayer coupling depends on the structural de-

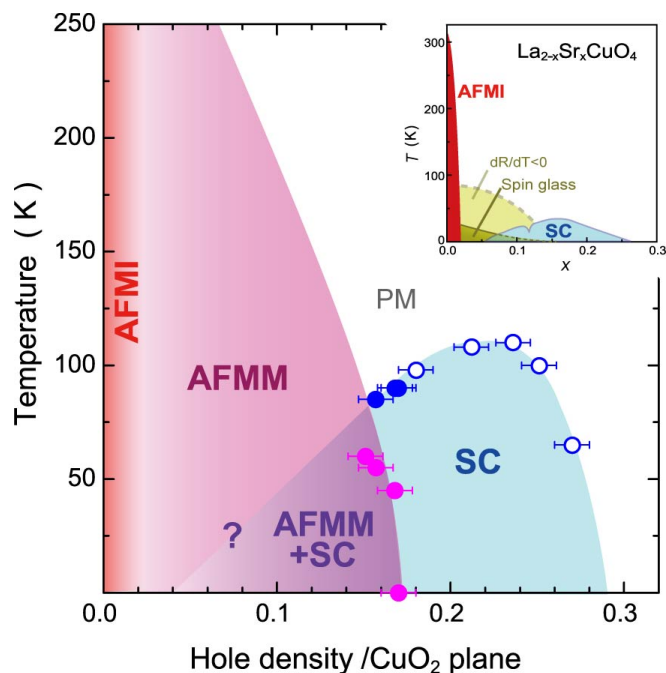


Fig. 8. (Color online) Phase diagram of homogeneously doped CuO_2 plane. On the basis of the results of various ve-layered cuprates, T_N and T_c are plotted as functions of N_h per CuO_2 plane determined only from the Knight shift. The solid and empty circles correspond to the data for IPs and OPs, respectively. It has been shown that (1) the AFM metallic (AFMM) phase is robust up to $N_h \approx 0.17$, (2) the uniformly mixed state of SC and AFMM is realized at least in $0.14 < N_h < 0.17$, (3) T_c has a peak close to the QCP at which the AFM order collapses, indicating the strong relationship between the high- T_c SC and AFM order. This phase diagram differs significantly from the well-established phase diagram of LSCO [cited from Ref.⁶] (see inset), in which both the phases are separated by the spin-glass phase in association with the carrier localization given by $d(\text{resistivity})/dT < 0$.

tails and number of CuO_2 planes. Assuming an isolated two-dimensional (2D) system, any long-range AFM order is not expected at a finite temperature. Therefore, this result reminds again that the interlayer coupling is crucial for the onset of AFM order. In a ve-layered system, three underdoped IPs may stabilize the long-range AFM order due to sufficient interlayer coupling. In this context, it is the weak interlayer magnetic coupling that suppresses the AFM order in LSCO⁶) and YBCO²⁰) at such small carrier densities region.

4.2 Proposal for understanding of underdoped state

As a result of the discussion above, we propose that the antiferromagnetically coupled spontaneous moment may persist up to $N_h \approx 0.16$ in the CuO_2 planes even in LSCO and YBCO as well, but may be hidden within the plane due to the strong 2D fluctuations brought about by the weak interlayer coupling. In fact, the application of a high magnetic field stabilizes the static AFM order in the vortex state in underdoped samples, but not in the optimally doped samples.^{23,24} Furthermore, the AFM order was also observed in the charge-stripe phases around $x = 1/8$ of LSCO.²⁵ As for the underdoped $\text{YBa}_2\text{Cu}_3\text{O}_{6.5}$ (YBCO 6.5) with $T_c = 60$ K, the AFM order has been

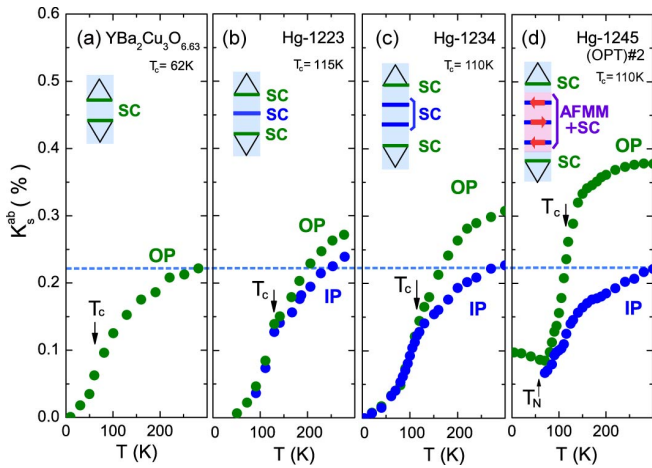


Fig. 9. (Color online) Knight shift for n -layered cuprates; (a) $n = 2$, $\text{YBa}_2\text{Cu}_3\text{O}_{6.63}$ ($T_c = 62 \text{ K}$) [cited from Ref.²¹]; (b) $n = 3$, Hg-1223 ($T_c = 115 \text{ K}$) [cited from Ref.¹⁴]; (c) $n = 4$, Hg-1234 ($T_c = 110 \text{ K}$); and (d) $n = 5$, Hg-1245 (OPT)\#2 . Although their carrier densities are almost N_h (OP or IP) = 0.16–0.01 evaluated from $K_s^{\text{ab}}(\text{RT}) \approx 0.22\%$ (dotted line), the ground state still remains paramagnetic for n -layered cuprates with $n = 4$. This suggests that three underdoped IPs in the case of $n = 5$ may stabilize the long-range AFM order due to sufficient interlayer coupling. We suggest that it is the two-dimensional fluctuations produced by the weak interlayer magnetic coupling that suppresses the AFM order in LSCO and YBCO by doping the small amount of holes.

reported in a neutron-scattering experiment, which suggested that an AFM moment of $0.1 \mu_B$ fluctuates in the nanosecond time scale.²⁶ In oxygen-ordered high-quality YBCO 6.5, a quantum oscillation revealed the Fermi surface comprising a Fermi pocket.²⁷ This result may be understood by assuming that the Fermi surface is folded at the magnetic Brillouin zone (Γ , Γ) due to the presence of the AFM order under a very high field. The Fermi arc observed in the photoemission spectra of underdoped cuprates²⁸ may also be explained by the Fermi pocket picture under the hidden short-range AFM order and by the collapse of a part of the Fermi surface caused by the very short lifetime of quasi-particles due to the disorder. Although the phase diagrams of LSCO and YBCO are widely believed thus far as typical phase diagram of cuprates, we claim that these underlying issues in their underdoped region may be affected by the strong 2D fluctuations produced by the weak interlayer coupling, in addition to the disorders caused by the chemical substitution for doping. This concept will lead us to a coherent understanding of underlying anomalies on underdoped cuprates, such as the AFM order induced by magnetic field,^{23,24} stripe order²⁵ in LSCO at $x = 1/8$, and the Fermi arc²⁸ in an underdoped region.

5. Conclusion

The site-selective NMR studies on the v -layered cuprates have unraveled the genuine phase diagram of the homogeneously doped CuO_2 plane: (1) the AFM order is robust up to $N_h \approx 0.17$, (2) the uniform mixing of AFM order and SC takes place at least in $0.14 < N_h < 0.17$, (3) T_c has a peak close to the QCP at which the AFM order collapses, and (4) the tetracritical point

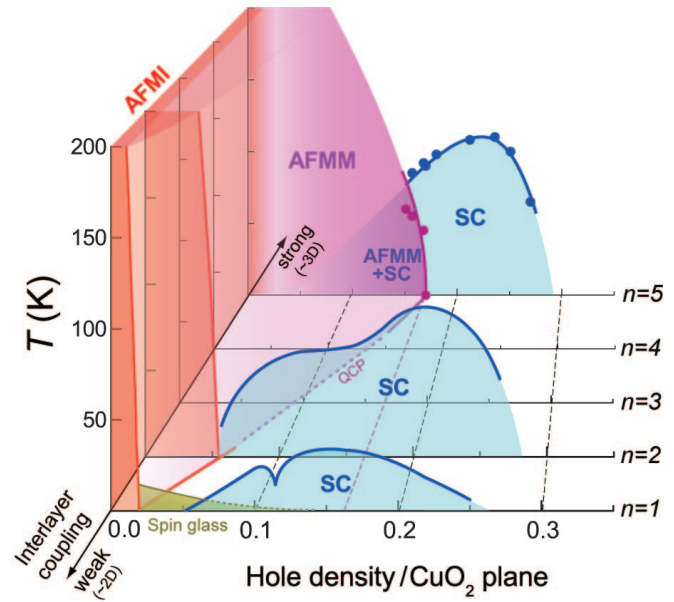


Fig. 10. (Color online) Comparison of phase diagrams for n -layered cuprates ($n = 5$). The phase diagram of v -layered cuprates differs from those of LSCO ($n = 1$) and YBCO ($n = 2$), in which the long-range AFM order collapses completely by doping with an extremely small amount of holes. In v -layered systems, three underdoped IPs may stabilize the long-range AFM order due to sufficient interlayer coupling, whereas the carrier density at QCP for n -layered systems with $n = 4$ becomes lower than that in v -layered systems because of the weak effective interlayer coupling that may suppress the AFM order. It strongly suggests that the QCP moves to a region of lower carrier density for n -layered cuprates with $n = 4$. Consequently, we consider that the antiferromagnetically coupled spontaneous moment may persist up to $N_h \approx 0.16$ for the CuO_2 planes in LSCO and YBCO also; however, it may be hidden within the plane due to the strong 2D fluctuations brought about by the weak interlayer coupling. This concept will lead us to a coherent understanding of underlying anomalies on underdoped cuprates (see text).

for the AFM / (AFM + SC) / SC / PM phases may be present at $N_h \approx 0.15$ and $T \approx 75 \text{ K}$. These results suggest the intimate relationship between the high- T_c SC and AFM order, namely, the AFM superexchange interaction plays a vital role not only for the onset of the AFM order but also of SC. Although the phase diagrams of LSCO and YBCO are widely believed thus far as typical ones, we claim that the underlying issues in underdoped LSCO, such as the stripe order, the magnetic-field-induced AFM order, Fermi arc, etc., may be affected by the disorder and/or by strong 2D fluctuations due to the weak interlayer coupling, in addition to the strong correlation effect. The results presented here allow us to obtain an insight that the AFM superexchange interaction is the most promising glue for the Cooper pair in cuprate superconductors.

Acknowledgement

We would like to thank M. Mori, T. Tohyama, S. Maezawa, H. Kohno and M. Ogata for their discussions. This work was supported by a Grant-in-Aid for Creative Scientific Research (15GS0213) from the Ministry of Education, Culture, Sports, Science and Technology (MEXT) and the 21st Century COE Program (G18) of

the Japan Society for the Promotion of Science (JSPS).

- 1) P.W. Anderson: The Theory of Superconductivity in the High- T_c Cuprate Superconductors (Princeton Univ. Press, 1997).
- 2) M. Inaba, H. Matsukawa, M. Saitoh and H. Fukuyama: Physica C 257, (1996) 299.
- 3) A. Himeda and M. Ogata: Phys. Rev. B 60 (1999) R9935.
- 4) E. Demler, W. Hanke, and S.C. Zhang: Rev. Mod. Phys. 76 (2004) 909.
- 5) T. Mori and K. Ueda: Rep. Prog. Phys. 66 (2003) 1299.
- 6) B. Keimer, N. Belk, R. J. Birgeneau, A. Cassanho, C. Y. Chen, M. G. Reven, and M. A. Kastner, A. Harony, Y. Endoh, R. W. Erwin, G. Shirane: Phys. Rev. B 46 (1992) 14034.
- 7) In this study, the IP in the central plane is also denoted as \bar{IP} because it is similar to the other IPs due to the carrier density and local environment being same.
- 8) Y. Tokunaga, K. Ishida, Y. Kitaoka, K. A. Sayama, K. Tokiwa, A. Iyo, and H. Ihara: Phys. Rev. B 66 (2000) 9707.
- 9) H. Kotehawa, Y. Tokunaga, K. Ishida, G.-q. Zheng, Y. Kitaoka, K. A. Sayama, H. Kito, A. Iyo, H. Ihara, K. Tanaka, K. Tokiwa, and T. Watanabe: Phys. Rev. B 64 (2001) 064515.
- 10) H. Kotehawa, Y. Tokunaga, Y. Arai, G.-q. Zheng, Y. Kitaoka, K. Tokiwa, K. Ito, T. Watanabe, A. Iyo, Y. Tanaka, and H. Ihara: Phys. Rev. B 69 (2004) 014501.
- 11) H. Mukuda, M. Abe, Y. Arai, Y. Kitaoka, K. Tokiwa, T. Watanabe, A. Iyo, H. Kito, and Y. Tanaka: Phys. Rev. Lett. 96 (2006) 087001.
- 12) H. Mukuda, M. Abe, S. Shimizu, Y. Kitaoka, A. Iyo, Y. Kodama, H. Kito, Y. Tanaka, K. Tokiwa, T. Watanabe: J. Phys. Soc. Jpn. 75 (2006) 123702.
- 13) K. Tokiwa, A. Iyo, T. Tsukamoto, and H. Ihara: Czech. J. Phys. 46 (1996) 1491.
- 14) M.-H. Julien, P. Carretta, M. Horvatic, C. Berthier, Y. Berthier, P. Segransan, A. Carrington, and D. Colson: Phys. Rev. Lett. 76 (1996) 4238.
- 15) K. M. Agishi, Y. Kitaoka, G.-q. Zheng, K. A. Sayama, K. Tokiwa, A. Iyo, and H. Ihara: J. Phys. Soc. Jpn. 64 (1995) 4561.
- 16) N. Kobayashi, Z. Hiroi, M. Takano: J. Sol. State Chem. 132 (1997) 274.
- 17) G.-q. Zheng, Y. Kitaoka, K. Ishida, K. A. Sayama: J. Phys. Soc. Jpn. 64 (1995) 2524.
- 18) D. Vaknin, S.K. Sinha, D.E. Moncton, D.C. Johnston, J.M. Newsam, C.R. Sanya, and H.E. King Jr.: Phys. Rev. Lett. 58 (1987) 2802.
- 19) M. Yashima, S.K. Awasaki, H. Mukuda, Y. Kitaoka, H. Shishido, R. Settai, and Y. Onuki: Phys. Rev. B 76 (2007) 020509(R).
- 20) S. Sanna, G. Allodi, G. Concas, A. Dhillier, and R. De Renzi: Phys. Rev. Lett. 93 (2004) 207001.
- 21) M. Takigawa, A.P. Reyes, P.C. Hammel, J.D. Thompson, R. Heber, Z. Fisk, and K.C. Ott: Phys. Rev. B 43 (1991) 247.
- 22) Y. Tokura, S. Koshihara, and T. Arita, H. Takagi, S. Ishibashi, T. Ido, and S. Uchida: Phys. Rev. B 41 (1990) 11657.
- 23) B. Lake, H.M. Ronnow, N.B. Christensen, G. Aeppli, K. Lefmann, D.F.M. Morrow, P. Vorderwisch, P. Smeyers-Verbeke, N. Mangkomtong, T. Sasagawa, M. Nohara, H. Takagi and T.E. Mason: Nature 415 (2002) 299.
- 24) R.I.M. Miller, R.F. Kiehl, J.H. Brewer, J.E. Sonier, J. Chakhalian, S. Dunsiger, G.D. Morris, A.N. Rice, D.A. Bonn, W.H. Hardy, and R. Liang: Phys. Rev. Lett. 88 (2002) 137002.
- 25) J.M. Tranquada, B.J. Stemlieb, J.D. Axe, Y. Nakamura, and S. Uchida: Nature 375 (1995) 561.
- 26) Y. Sidis, C. Ulrich, P. Bourges, C. Bernhard, C. Niedermayer, L.P. Regnault, N.H. Andersen, and B. Keimer: Phys. Rev. Lett. 86 (2001) 4100.
- 27) N. Doiron-Leyraud, C. Proust, D. LeBoeuf, J. LeVallois, J. Bonnemaison, R. Liang, D.A. Bonn, W.H. Hardy and L. Taillefer: Nature 447 (2007) 565.
- 28) M.R. Norman, H. Ding, M. Randeria, J.C. Campuzano, T. Yokoya, T. Takeuchi, T. Takahashi, T. Mochiku, K. Kadowaki, P. Guptasama, and D.G. Hinks: Nature 392 (1998) 157.